

ARTICLE OPEN



Chitosan-based fluorescent inverse opal particles for Cr(VI) sensing

Haiwen Su¹, Hong Chen², Baojie Wen², Ling Lu², Dagan Zhang² and Huan Wang^{1,3}

Chitosan (CS) is a natural polymer widely used in many fields. However, there are seldom studies that focus on its inherent fluorescence properties. In this work, based on the inherent fluorescence of chitosan (CS) and the mechanism that it can be quenched by hexavalent chromium (Cr(VI)), we developed novel CS-based inverse opal particles (IOPs) for Cr(VI) detection. The CS IOPs were obtained by replicating the silica colloidal crystal beads using CS, which displayed uniform shape and size, as well as enhanced fluorescence-emission capability resulted from the unique microstructure. Under the optimized conditions, the CS IOPs responded to Cr(VI) in a range of 0–10,000 μM with high sensitivity and specificity and demonstrated a LOD of 0.055 μM at the linear range of 0–30 μM . Furthermore, they displayed good detection ability in practical applications with recoveries of 86–106% for tap water and 99.7–107.3% for pond water, respectively. With these features, the developed CS IOPs are promising to be a simple, low-cost, and fast platform for detecting Cr(VI).

npj Clean Water (2023)6:70; <https://doi.org/10.1038/s41545-023-00283-5>

INTRODUCTION

Chromium and its compounds are widely used in many fields, such as alloy, dyestuff, leather tanning, electroplating, and catalysis^{1–5}, which causes wide pollution of toxic chromium in soil and water environments^{6,7}. The recommended value of total chromium in drinking water is 0.96 μM (0.05 mg/L) by the World Health Organization (WHO)⁸. However, chromium mainly exists in trivalent (Cr(III)) and hexavalent (Cr(VI)), while the latter is about 100 times more toxic than the former and is on the list of Class I carcinogens⁹. Therefore, the determination of total chromium can not reveal the actual impacts on health and the environment, while the assay of Cr(VI) is meaningful and crucial. Various strategies have been developed for Cr(VI) detection, including spectrophotometry¹⁰, inductively coupled plasma-atomic emission spectrometry¹¹, inductively coupled plasma mass spectrometry¹², atomic absorption spectroscopy¹³, electrochemistry¹⁴, and fluorescence^{15–19}. Though these methods have high sensitivity and selectivity, the complex sample pretreatment, demand of expensive equipment, tedious preparation processes, as well as time-consuming process limit their further applications. Hence, a new simple, cheap, and fast method for Cr(VI) detection is still anticipated.

Herein, we present simple chitosan (CS) inverse opal particles (IOPs) for Cr(VI) assay (Fig. 1). CS is a natural polymer derived from chitin with abundant amino groups and is widely used in the biomedical field^{20–31}. Interestingly, it shows fluorescence under the irradiation of excitation light^{32–37}, and it maintains after covalently binding with glutaraldehyde (GA)^{38–40}, and the fluorescence can be quenched by Cr(VI). This phenomenon might be attributed to the fact that the Cr(VI) can bind the CS and quench the fluorophores of the nonconjugated CS⁴⁰, and thus, this mechanism could be a possible method for Cr(VI) detection. Compared with other reported Cr(VI) assay strategies, CS-based fluorescent detection has the advantages of simple assay

operation and the abundant source from the nature of CS, which results in low-cost. Nevertheless, the low crosslinking degree or bulk structure of the CS-GA leads to nonuniform and incomplete reactions as well as significant demand for raw materials and samples. In contrast, inverse opals are materials with three-dimensional (3D) macropores^{41–48}. They can be easily acquired by replicating 3D colloidal crystal templates and inherit the ordered microstructure and photonic properties^{49–54}. Moreover, when inverse opals are composed of responsive hydrogels, they can respond to corresponding stimuli and be regarded as biosensors. Particularly, IOPs are extremely popular because of their high homogeneity, moveability, controllability, smaller volume, and larger specific surface area^{55–58}. Although various IOPs have been prepared for biosensing^{59–63}, seldom of them could assay Cr(VI) level in the water, and CS IOPs for Cr(VI) sensing via simple fluorescence quenching have not been reported yet.

In this work, we presented CS IOPs by simply replicating the silica colloidal crystal beads (SCCBs) generated from microfluidics. Due to the precise control of the microfluidic platform, the SCCBs displayed uniform size, and IOPs inherited it. Besides, the CS component endowed IOPs with a fluorescence feature, which was stable in wide pH and temperature ranges for a long time. Moreover, benefiting from the fluorescence enhancement of the photonic structure, the IOPs showed stronger fluorescent intensity than pure CS particles of the same size. When the IOPs were immersed in the Cr(VI) solution, the fluorescence could be quenched by Cr(VI) within several minutes, while it was relatively stable in the solution of other ions. The results showed that the quenching ratio increased linearly in the concentration range of Cr(VI) of 1–30 μM and has a limit of detection (LOD) of 0.055 μM . The practical application in detecting the Cr(VI) within tap water was also performed by the standard addition method. With these features, the developed CS IOPs are promising to be a simple and cheap platform for the fast, sensitive, and specific Cr(VI) detection.

¹The Eighth Affiliated Hospital, Sun Yat-Sen University, 518033 Shenzhen, China. ²Department of Otolaryngology Head and Neck Surgery, Jiangsu Provincial Key Medical Discipline, Nanjing Drum Tower Hospital, Affiliated Hospital of Medical School, Nanjing University, 210008 Nanjing, China. ³Guangdong Key Laboratory for Biomedical Measurements and Ultrasound Imaging, Department of Biomedical Engineering, Shenzhen University, 518060 Shenzhen, China. ✉email: entluling60@126.com; zhang_dagan@126.com; wangh679@mail.sysu.edu.cn

RESULTS AND DISCUSSION

Design and characterization of CS IOPs

In a typical experiment, SCCBs were prepared in advance and used as templates for IOPs. Briefly, the silica nanoparticle droplets generated from a microfluidic platform were heated in an oven to evaporate water and induce the self-assembly of nanoparticles to form SCCBs. Benefitting from the precise controllability of fluids by the microfluidic platform, the SCCBs displayed uniform size^{64–69}. The SCCBs were calcined after washing from silicon oil to acquire better mechanical strength. Then the SCCBs were immersed in CS pregel to allow the pregel to permeate into the nanovoids within the SCCBs. After polymerization, the SCCB/CS hybrid particles were obtained, and the silica nanoparticles within the hybrid particles could be removed by HF and thus, IOPs were prepared. Nevertheless, the pure CS IOPs were highly transparent

in water and hard to be observed (Supplementary Fig. 1a). To address this problem, polyethylene glycol diacrylate (PEGDA) was doped into the pregel and used in the following experiments (Supplementary Fig. 1b).

To observe the microstructure change of the particles during the fabrication process, a scanning electron microscope (SEM) was applied. As shown in Fig. 2a, b and Supplementary Fig. 2a, an SCCB exhibited an excellent spherical shape, and the nanoparticles on the surface of the obtained SCCBs assembled into a closely packed form, and this structure extended into the inside. Meanwhile, there were many nanovoids among the nanoparticles, which could be filled with CS solution. When the solution was gelled, the voids were filled with CS hydrogel, and SCCB/CS hybrid particles were realized (Fig. 2c, d). After the removal of the silica nanoparticles, CS IOPs were prepared. However, the hydrogel

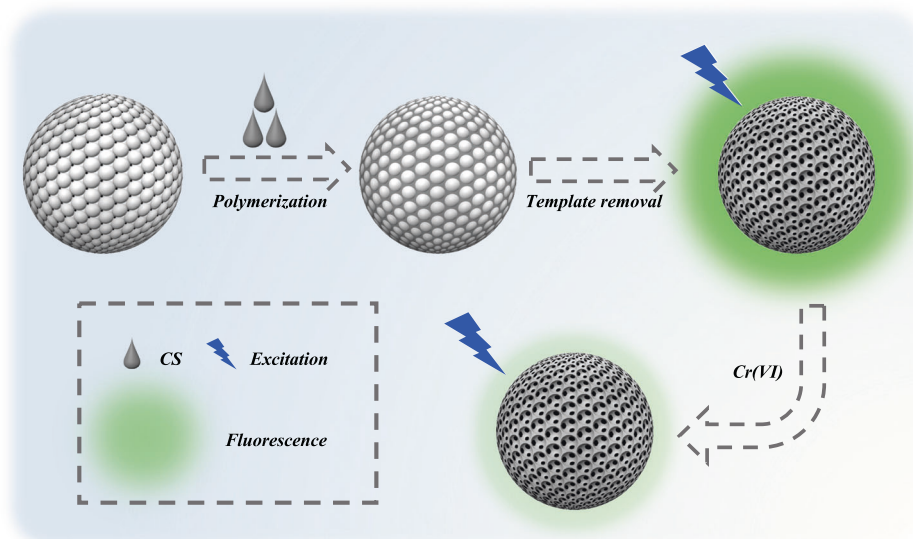


Fig. 1 Schematic diagram. The fabrication of CS IOPs and the mechanism for Cr(VI) detection.

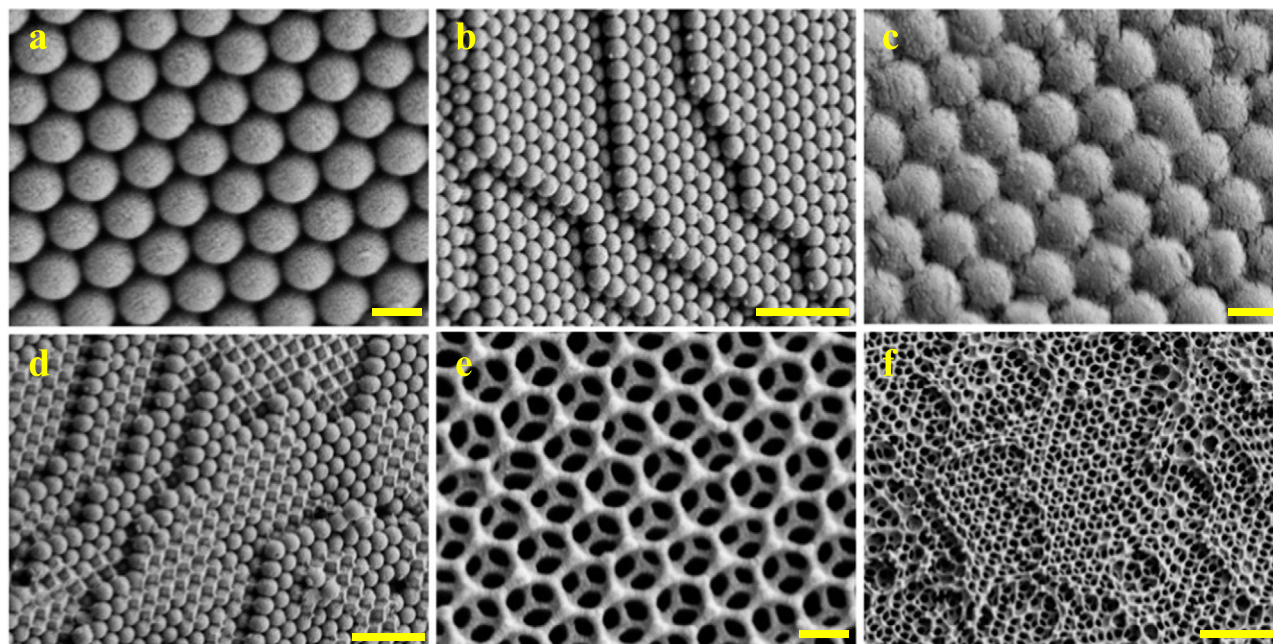


Fig. 2 SEM characterization of SCCBs and IOPs. The surface and inside microstructure of an SCCB (a, b), an SCCB/CS hybrid particle (c, d), and an IOP particle (e, f). Scale bars are 200 nm in a, c, e, and 1 μm in b, d, f.

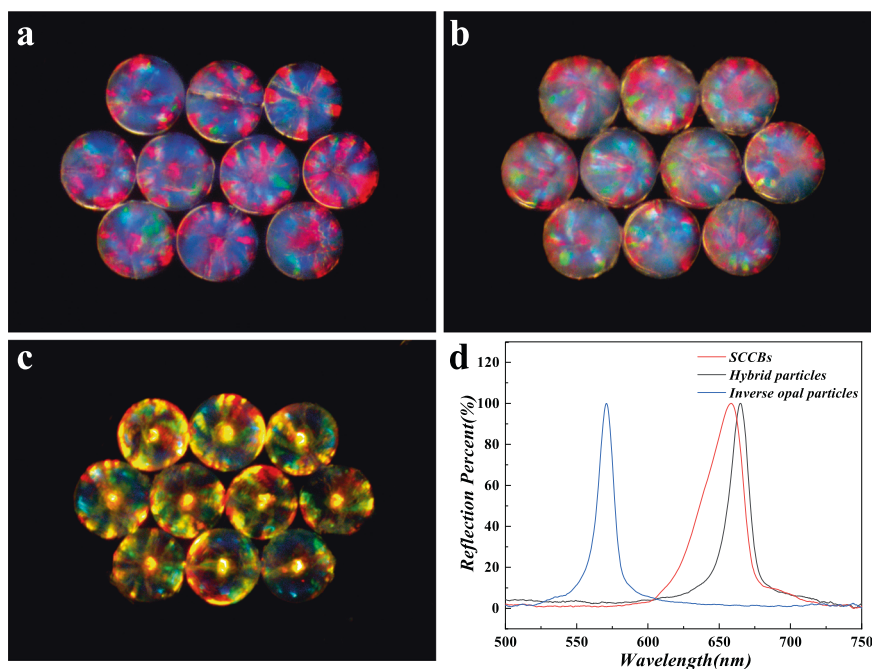


Fig. 3 Optical characterization of the particles. **a–c** The image of SCCBs with reflective peaks at 660 nm (**a**) and their corresponding SCCB/CS hybrid particles (**b**) and CS IOPs (**c**). **d** The reflective spectra of the particles in **a–c**.

network's strength was relatively weak and often collapsed during drying (Supplementary Fig. 2b). Therefore, a pregel with a high crosslinker concentration was employed to reveal the microstructure of IOPs. As expected, the IOP had an orderly inverse opal microstructure complementary to the SCCB (Fig. 2e, f).

It is worth noting that the ordered microstructure endowed the SCCBs with structural color properties, which result from the photonic bandgap (PBG). As described in many works before, the reflective peak λ of SCCB was mainly determined by the refractive index and lattice spacing, and the value can be approximately estimated as^{70,71}:

$$\lambda = 1.633dn_{\text{average}} \quad (1)$$

where d and n_{average} refer to the diameter of the nanoparticles and the average refractive index, respectively. Since the average refractive index is the same when the raw materials and packing forms are constant, the color of SCCBs is mainly dependent on d , i.e., by choosing nanoparticles of different sizes, SCCBs with various colors can be prepared. Moreover, the hybrid particles and IOPs derived from SCCBs inherited the structural colors that depended on the size of the nanoparticles of the SCCB templates (Fig. 3; Supplementary Figs. 3 and 4). The hybrid particles generally had a slight red-shifted reflective peak than SCCBs because the filled hydrogel had a higher refractive index than water. In contrast, the CS IOPs showed a sharp blue shift, which could be attributed to replacing high-refractive index silica with low-refractive-index water.

Optimization of hydrogel concentration ratio

Before using CS IOPs for Cr(VI) detection, we optimized the concentrations of CS and PEGDA. As shown in Supplementary Fig. 5, the fluorescence intensity of CS IOPs enhanced with the increase of CS concentration, while it was weakened with the rise of PEGDA concentration. These results could be attributed to the fact that the fluorescence was emitted from CS, the more CS there were, the more fluorescence there was. Meanwhile, PEGDA might hinder the interaction of the CS network and affect the fluorescence generation mechanism. However, the CS solution with higher concentrations might dissolve insufficiently and inhomogeneously, while lower PEGDA concentration led to

increased transparency and poor mechanical strength. Therefore, we employed 4% (w/v) CS and 10% (v/v) PEGDA as the compromised concentration to prepare pregel for the subsequent experiments.

CS IOPs for Cr(VI) detection

To verify the Cr(VI) detection capability, CS IOPs were immersed in Cr(VI) solution with different concentrations, respectively. As shown in Fig. 4a, though the CS IOPs displayed inherent fluorescence in all the solutions, the intensity was weakened with the increasing Cr(VI) concentration within several minutes (Supplementary Fig. 6), which could be ascribed to the Cr(VI)'s quenching effect. The further quantitative fluorescence intensity change was shown in Fig. 4b, c. It could be found that the pure PEGDA IOPs showed no fluorescence in all kinds of Cr(VI) solutions. In contrast, the CS IOPs exhibited fluorescence quenching to Cr(VI) with concentrations from 1 to 10,000 mM. In the range from 0 to 30 μM , the results showed excellent linear change ($R^2 = 0.99617$, measurement uncertainty 0.07676) and a LOD of 0.055 μM . Compared with other strategies reported in Table 1, such as photoelectrochemistry, voltammetry, colorimetry, and fluorescence, the presented CS IOPs had an acceptable linear range and the lowest LOD among the fluorescence methods. Coupled with the more straightforward and less expensive operation and the short time, the presented CS IOPs are possible to be a reliable alternative.

Theoretically, the CS hydrogel particles without inverse opal structure could also be used for Cr(VI) detection. However, it was hard to generate GA-crosslinked CS particles with uniform size and shape due to the fast gelation time. Although the stirring method could form some CS particles, the poor size dispersion and shape consistency might cause massive variation in the results (Supplementary Fig. 7). In addition, the CS particles displayed lower fluorescence intensity than CS IOP particles replicated from the green SCCBs of the same size (Supplementary Fig. 8a). However, compared with CS particles, there was less CS content in the CS IOPs because the inverse opal structure only has a duty ratio of 26%. This result might be attributed to the fluorescence-emission enhancement effect caused by the inverse

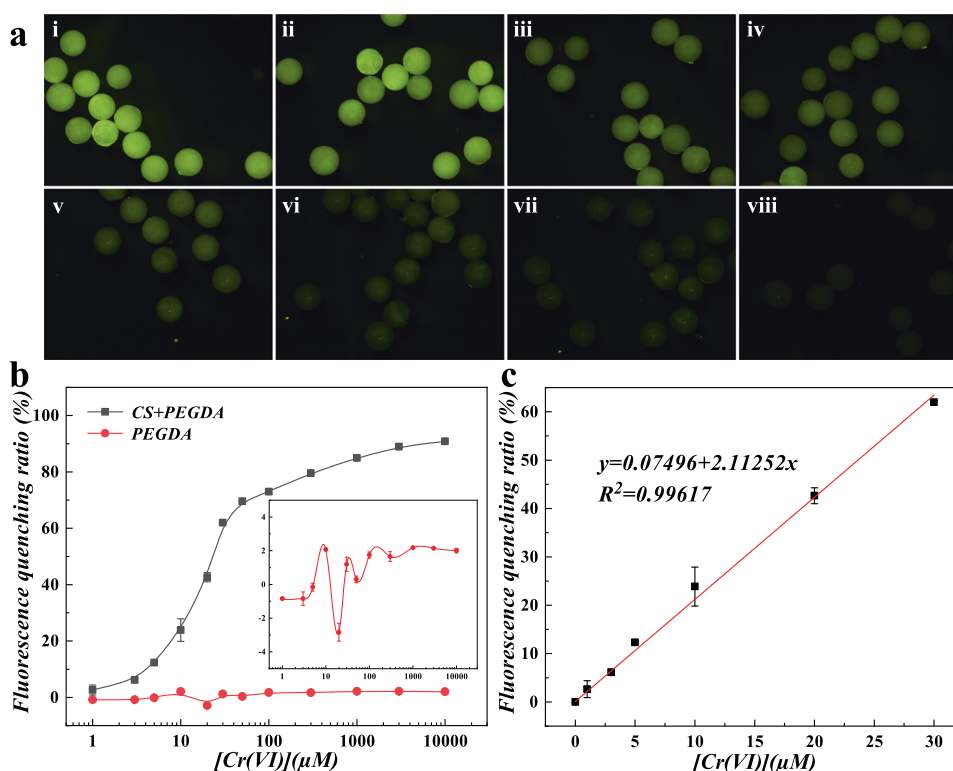


Fig. 4 **Cr(VI) detection capability of CS IOPs.** **a** The fluorescent image of CS IOPs in Cr(VI) solution with concentrations of 0, 3, 20, 30, 50, 300, 1000, and 10,000 μM (i–viii), respectively. **b** The relative fluorescence quenching of CS IOPs and PEGDA IOPs in Cr(VI) solution with various concentrations, respectively. **c** The relative fluorescence quenching of CS IOPs in Cr(VI) solution with concentrations of 0–30 μM and the corresponding linear fitting curve. The number of replications in each group was 3, and the error bars were standard deviations.

Table 1. Overview of recently reported Cr(VI) sensors.

Sensors	Methods	Linear range (μM)	The detection limit (μM)	Ref.
BiVO ₄ -7	Photoelectrochemistry	2–210	0.01	74
TiO ₂ /graphene/ gold	Photoelectrochemistry	0.027–49.852	0.008	75
AuNPs–BDD electrode	Voltammetry	0.19–19.23	0.023	76
Ox -MWCNT-Au	Voltammetry and amperometry	0.8–230	0.72	77
Au NDC@Ag NRs	Colorimetry	2.5–40	1.69	78
R-CuO-TMB /dopamine system	Colorimetry	2–10	0.47	79
DECQDs	Fluorescence and colorimetry	5.3–320	1.6	80
CCDs	Fluorescent spectrum	5–125	1.17	81
r-CD	Fluorescence	1.98–250	0.9	82
CS IOP	Fluorescence	1–30	0.055	This work

opal structure^{72,73}. The PBG edge of CS IOPs was close to the emission band of CS fluorescence and increased the intensity remarkably. According to the particles' fluorescence intensity and CS content, the inverse opal structure enhanced the fluorescence intensity by about 580%. More interestingly, owing to the ordered macropore structure, CS IOPs demonstrated higher sensitivity than CS particles (Supplementary Fig. 8b). These features indicated that the microstructure of CS IOP played an essential role in Cr(VI) assay. It is worth noting that the practical detecting conditions are often complex, the temperature, pH, and impurity ions content are quite different in the samples under diverse working environments. To investigate the fluorescence stability of CS IOPs, we treated the CS IOPs in various conditions. As shown in Supplementary Fig. 9a, the CS IOPs kept relatively stable fluorescence intensity when the pH value changed from 3 to 9,

indicating they were useful in most water samples. In contrast, CS IOPs demonstrated a little weakened fluorescence intensity when the temperature was higher than 40 °C (Supplementary Fig. 9b). This might have a negligible effect on detection because most water samples from the natural environment were lower than 40 °C. In addition, the storage time of CS IOPs was also studied, which showed little influence on the fluorescence intensity (Supplementary Fig. 9c). Although the repeatability was relatively poor (Supplementary Fig. 10), it could be overcome by the high yield (3×10^4 droplets per hour). These results indicated that the CS IOPs are stable and useful in most work conditions.

The specificity and anti-interference properties of CS IOPs were also confirmed. Typically, the CS IOPs were incubated in a 1 mM solution of various ions for 10 min, and then assaying their fluorescence intensity. To enable a visual comparison, the

fluorescence intensity of CS IOPs before and after incubation was set as F_0 and F , respectively. As shown in Fig. 5a, c, the interferent ions caused fluorescence quenching smaller than 4%, while Cr(VI) weakened the fluorescence intensity by more than 80% at the same concentration (Fig. 4b). We further investigated the interference effects of these ions in the solution containing Cr(VI) by adding 1 mM interferent ions into 20 μM Cr(VI). As shown in Fig. 5b, d, the CS IOPs in all the groups exhibited remarkable fluorescence quenching. The deviations caused by various interferent ions were less than 5%, even though the concentrations of interferent ions were 50-fold higher than Cr(VI). It was noted that ethylenediamine tetraacetic acid disodium (EDTA-2Na) was employed as the masking reagent in the detection. When it was absent in the solution, the interferent metal cations strongly influenced the fluorescence intensity, as shown in Supplementary

Fig. 10. This might be attributed to the added EDTA that chelated the interferent metal cations, which could bind with the CS and cause unexpected fluorescence changes.

Application of CS IOPs in real samples

The practical application of CS IOPs was investigated by assaying the Cr(VI) content in tap water by spiking standard samples. The fluorescence intensity of CS IOPs was analyzed and transformed into Cr(VI) concentrations. As shown in Fig. 6, Tables 2 and 3, the Cr(VI) concentrations of tap water and pond water were determined as 0.066 μM , and 0.186 μM , respectively, and the CS IOPs had good recoveries of 86–106% for tap water and 99.7–107.3% for pond water, respectively, indicating the developed CS IOPs were reliable in practical Cr(VI) analysis.

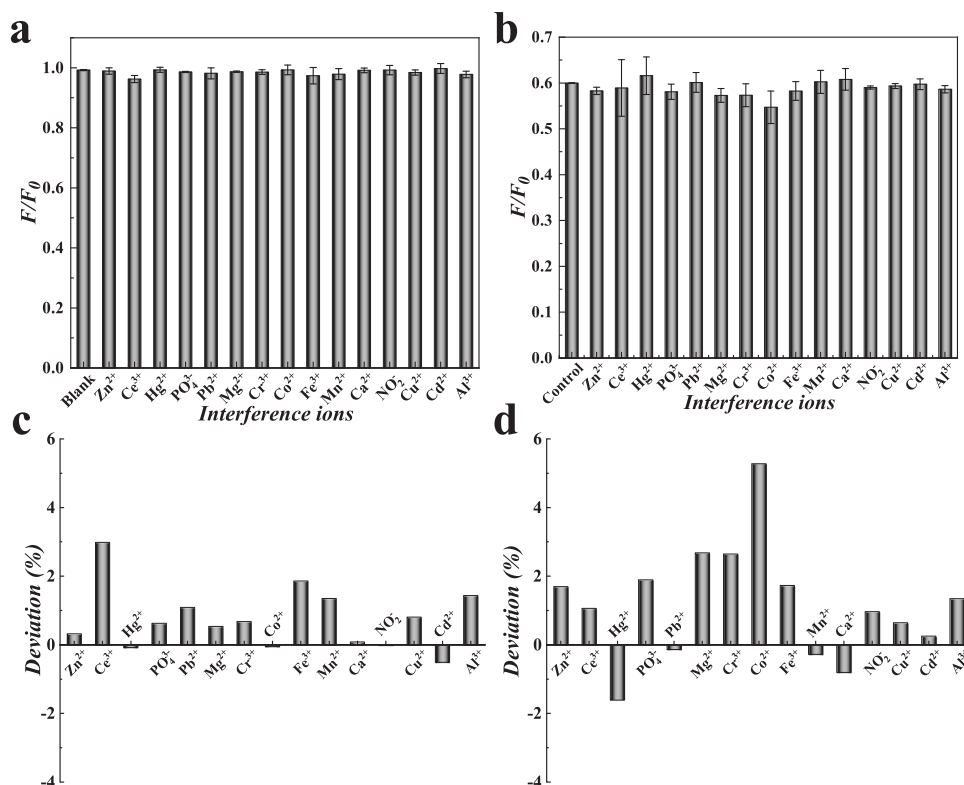


Fig. 5 Anti-interference performance of CS IOPs. **a** The fluorescence intensity changes of CS IOPs in different interferent ion solutions. **b** The fluorescence intensity changes of CS IOPs in 20 μM Cr(VI) solution with 1 mM interferent ions. **c, d** The deviations caused by the interferent ions in **a** and **b**. The number of replications in each group was 3, and the error bars were standard deviations.

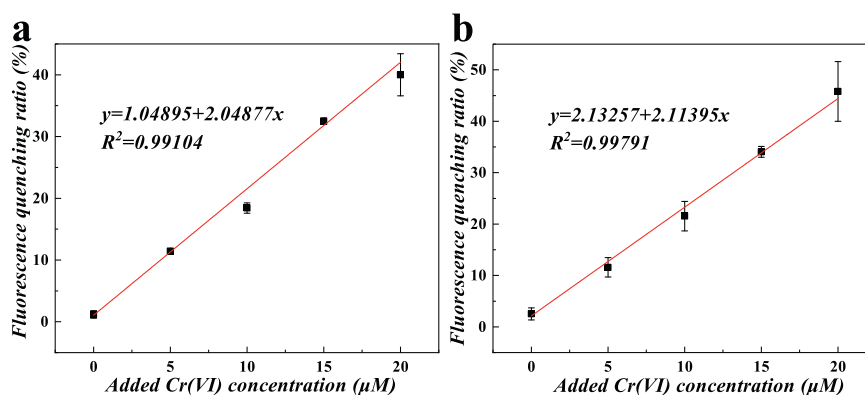


Fig. 6 The practical application of CS IOPs in real samples. The tap water (**a**) and pond water (**b**) were accomplished by spiking standard samples. The number of replications in each group was 3, and the error bars were standard deviations.

Table 2. Detecting Cr(VI) in tap water using CS IOPs.

Added (μM)	Found in tap water (μM)	RSD(%)	Recovery (%)
5	5.30	2.73	106
10	8.60	4.53	86
15	15.27	1.59	100.9
20	18.82	8.55	94.1

Table 3. Detecting Cr(VI) in pond water using CS IOPs.

Added (μM)	Found in pond (μM)	RSD(%)	Recovery (%)
5	5.26	16.50	105.2
10	9.97	13.33	99.7
15	15.89	3.10	105.9
20	21.46	12.72	107.3

In summary, we developed the novel CS IOPs for Cr(VI) detection based on the inherent fluorescent property of CS. The CS IOPs had uniform shape and size, and the unique microstructure enhanced the fluorescence-emission capability of CS. When immersed in the solution, they could assay Cr(VI) concentration in a range of 0–10,000 μM with high sensitivity and specificity and had a LOD of 0.055 μM at the 0–30 μM linear range. The applicability of CS IOPs was also confirmed by assaying tap water and pond water. We believe this work can provide a simple, low-cost, and time-saving approach for Cr(VI) determination and inspire researchers that solve challenges by simple methods and common materials.

Although the CS IOPs have distinct advantages, some aspects of the detection system are worth improving. First, the linear range of current CS IOPs is relatively small, it's better to acquire a larger range for wide application scenarios. Second, the sample solutions should be pretreated before detecting by the CS IOPs, which increases the workload. Third, the CS IOPs can only recognize Cr(VI) with high sensitivity and specificity, while there are many more types of heavy metal ions in the environment that should be monitored. With these subsequent efforts, the CS IOPs are expected to open a new route in environment monitoring.

METHODS

Materials

Chitosan (CS, deacetylation degree 80–95%, 50–800 mPa·s), ethylenediamine tetraacetic acid disodium (EDTA·2Na), Na_2CrO_4 , Na_3PO_4 , NaNO_2 , $\text{Cr}(\text{NO}_3)_3$, $\text{Ce}(\text{NO}_3)_3$, $\text{Fe}(\text{NO}_3)_3$, $\text{Hg}(\text{NO}_3)_2$, $\text{Al}(\text{NO}_3)_3$, $\text{Mg}(\text{NO}_3)_2$, $\text{Co}(\text{NO}_3)_2$, $\text{Mn}(\text{NO}_3)_2$, $\text{Ca}(\text{NO}_3)_2$, $\text{Cu}(\text{NO}_3)_2$, $\text{Cd}(\text{NO}_3)_2$, and $\text{Zn}(\text{NO}_3)_2$ were bought from Shanghai Sinopharm Co., Ltd. 2-hydroxy-2-methylpropiophenone photoinitiator (HMPP) and poly(ethylene glycol) diacrylate (PEGDA, Mw 700) were obtained from Sigma-Aldrich. Glutaraldehyde (GA), hydrofluoric acid (HF, 40%, v/v), Paraffin liquid, and acetic acid were acquired from Macklin. All the reagents were analytical grade or higher and used as received. Water was purified and with a resistivity higher than 18M Ω ·cm.

Preparation of SCCBs

SiO_2 nanoparticles were dispersed in water to form a solution (20%, w/v), which was utilized as the inner phase (1 mL/h) and cut into droplets by silicon oil (500 cSt, 6 mL/h) using a single-emulsion microfluidic platform. The droplets were collected and dried in an oven (75 °C) overnight. After that, the dried SCCBs were

washed with n-hexane to remove silicon oil. Finally, the beads were calcined by a muffle furnace at 800 °C for 4 h to enhance mechanical strength.

Fabrication of chitosan inverse opal particles (CS IOPs)

To fabricate CS IOPs, the SCCBs were immersed in the solution containing CS, PEGDA, and HMPP (1%) for 6 h to ensure the solution infiltrated into the nanovoids of SCCBs. After that, the system was polymerized by ultraviolet (UV) light. Then, the SCCB/CS hybrid particles were stripped manually and treated with GA (5%, v/v) for 4 h to crosslink the CS. Finally, HF was employed to remove the SCCBs templates and obtain the CS IOPs. By changing the concentration of CS (1, 2, 3, and 4%, w/v) and PEGDA (0, 5, 10, 15, and 20%, v/v), a series of CS IOPs were developed. Meanwhile, the pure CS particles were prepared by dropwise adding the fresh mixing solution of CS (800 μL , 4%, w/v) and GA (200 μL , 5%, v/v) into the liquid paraffin containing Span 80 (10%, w/v) and constantly stirring (800 rpm) at 50 °C.

Detection of Cr(VI) using CS IOPs

CS IOPs were employed and pictured under a fluorescence microscope before detection. Then, they were immersed in the Na_2CrO_4 solution (0, 1, 3, 5, 10, 20, 30, 50, 100, 300, 1000, 3000, and 10,000 μM , respectively) containing EDTA (2 mM) for 10 min. After that, the CS IOPs were washed gently and pictured under a fluorescence microscope again. The average fluorescence intensities of CS IOPs before and after incubation were analyzed by Image J.

The specificity property of CS IOPs

CS IOPs were employed and pictured under a fluorescence microscope before detection. Then, they were immersed in different ion solutions with a concentration of 1 mM containing EDTA (2 mM) for 10 min. After that, the CS IOPs were washed gently and pictured under a fluorescence microscope again. The average fluorescence intensities of CS IOPs before and after incubation were analyzed by Image J.

The anti-interference property of CS IOPs

CS IOPs were employed and pictured under a fluorescence microscope before detection. Then, they were immersed in Na_2CrO_4 solution (20 μM) with different interferent ion solutions (1 mM) containing EDTA (2 mM) for 10 min. After that, the CS IOPs were washed gently and pictured under a fluorescence microscope again. The average fluorescence intensities of CS IOPs before and after incubation were analyzed by Image J.

Detection of Cr(VI) in tap water using CS IOPs

The Cr(VI) concentration in tap water was determined by the spiking method. CS IOPs were employed and pictured under a fluorescence microscope before detection. Then, they were immersed in the tap water containing different added concentrations of Na_2CrO_4 solution (0, 5, 10, 15, and 20 μM , respectively) containing EDTA (2 mM) for 10 min. After that, the CS IOPs were washed gently and pictured under a fluorescence microscope again. The average fluorescence intensities of CS IOPs before and after incubation were analyzed by Image J.

DATA AVAILABILITY

The authors declare that the data supporting the findings of this study are available within the paper and its supplementary information files.

Received: 14 April 2023; Accepted: 16 October 2023;
Published online: 30 October 2023

REFERENCES

- Jiang, Z. et al. Filling metal-organic framework mesopores with TiO₂ for CO₂ photoreduction. *Nature* **586**, 549–554 (2020).
- Xie, Y. et al. A percolation theory for designing corrosion-resistant alloys. *Nat. Mater.* **20**, 789–793 (2021).
- Zhang, B. et al. Atomically dispersed chromium coordinated with hydroxyl clusters enabling efficient hydrogen oxidation on ruthenium. *Nat. Commun.* **13**, 5894 (2022).
- Dutta, S. et al. Chromium/photoredox dual catalyzed synthesis of alpha-benzylic alcohols, isochromanones, 1,2-oxy alcohols and 1,2-thio alcohols. *Angew. Chem. Int. Ed.* **61**, e202212136 (2022).
- Kreider, M. E. et al. Understanding the stability of manganese chromium antimonate electrocatalysts through multimodal in situ and operando measurements. *J. Am. Chem. Soc.* **144**, 22549–22561 (2022).
- Zhang, J. et al. Polystyrene microplastics reduce Cr(VI) and decrease its aquatic toxicity under simulated sunlight. *J. Hazard. Mater.* **445**, 130483 (2022).
- Zhou, Z. et al. Iron-modified biochar-based bilayer permeable reactive barrier for Cr(VI) removal. *J. Hazard. Mater.* **439**, 129636 (2022).
- World Health Organization. *Guidelines for Drinking-water Quality, 4th Edition, Incorporating the 1st Addendum*. (World Health Organization, 2017).
- An, Y. et al. A dual-readout paper-based analytical device for the simultaneous determination of hexavalent Cr and total Cr. *Microchim. Acta* **189**, 445 (2022).
- Noroozifar, M. & Khorasani-Motlagh, M. Specific extraction of chromium as tetrabutylammonium-chromate and spectrophotometric determination by diphenylcarbazide: Speciation of chromium in effluent streams. *Anal. Sci.* **19**, 705–708 (2003).
- Sumida, T. et al. On-line preconcentration using dual mini-columns for the speciation of chromium(III) and chromium(VI) and its application to water samples as studied by inductively coupled plasma-atomic emission spectrometry. *Talanta* **68**, 388–393 (2005).
- Guerrero, M. M. L. et al. On-line preconcentration using chelating and ion-exchange minicolumns for the speciation of chromium(III) and chromium(VI) and their quantitative determination in natural waters by inductively coupled plasma mass spectrometry. *J. Anal. Atom. Spectrom.* **27**, 682–688, (2012).
- Kamakura, N., Inui, T., Kitano, M. & Nakamura, T. Determination of chromium(III), chromium(VI), and chromium(III) acetylacetonate in water by ion-exchange disk extraction/metal furnace atomic absorption spectrometry. *Spectrochim. Acta B* **93**, 28–33 (2014).
- Metters, J. P., Kadara, R. O. & Banks, C. E. Electroanalytical sensing of chromium(III) and (VI) utilising gold screen printed macro electrodes. *Analyst* **137**, 896–902 (2012).
- Xie, J. et al. Green synthesis of carbon quantum dots derived from lycium barbarum for effective fluorescence detection of Cr(VI) sensing. *J. Fluoresc.* <https://doi.org/10.1007/s10895-023-03300-5> (2023).
- Jia, K. et al. One-step fabrication of dual functional Tb(3+) coordinated polymeric micro/nano-structures for Cr(VI) adsorption and detection. *J. Hazard. Mater.* **423**, 127166 (2022).
- Musikavanhu, B. et al. Turn-off detection of Cr(III) with chelation enhanced fluorescence quenching effect by a naphthyl hydrazone Schiff base chemosensor. *Spectrochim. Acta A Mol. Biomol. Spectrosc.* **281**, 121599 (2022).
- Tawfik, S. M. et al. Blue-green emitting cationic thiazole surfactants-based paper devices for highly sensitive and selective fluorescence detection of chromium oxyanions in wastewater. *Microchem. J.* **193**, 108988 (2023).
- Busayaporn, W. et al. Synthesis and application of fluorescent N-doped carbon dots/hydrogel composite for Cr(VI) adsorption: Uncovering the ion species transformation and fluorescent quenching mechanism. *Environ. Geochem. Health* **45**, 5293–5309 (2023).
- Ahmed, M. et al. Recent developments in hazardous pollutants removal from wastewater and water reuse within a circular economy. *npj Clean Water* **5**, 12 (2022).
- Tran, L. B. et al. Advanced natural hydrated iron-alum oxides cation exchange resin for simultaneous phosphate and hardness removal. *npj Clean Water* **5**, 43 (2022).
- Alsawy, T., Rashad, E., El-Qelish, M. & Mohammed, R. H. A comprehensive review on the chemical regeneration of biochar adsorbent for sustainable wastewater treatment. *npj Clean Water* **5**, 29 (2022).
- Wang, H. et al. Polymer-based responsive structural color materials. *Prog. Mater. Sci.* **135**, 101091 (2023).
- Wang, H. et al. Injectable hydrogels for spinal cord injury repair. *Eng. Regen.* **3**, 407–419 (2022).
- Chen, C. et al. Multifunctional chitosan inverse opal particles for wound healing. *ACS Nano* **12**, 10493–10500 (2018).
- Wang, J. et al. Developing tissue engineering strategies for liver regeneration. *Eng. Regen.* **3**, 80–91 (2022).
- Hu, Y. et al. Scaffolds with anisotropic structure for neural tissue engineering. *Eng. Regen.* **3**, 154–162 (2022).
- Ma, Y. et al. Spinal cord conduits for spinal cord injury regeneration. *Eng. Regen.* **4**, 68–80 (2023).
- Qiu, L., Kong, B., Kong, T. & Wang, H. Recent advances in liver-on-chips: Design, fabrication, and applications. *Smart Med.* **2**, 20220010 (2023).
- Kong, B. et al. Tissue adhesives for wound closure. *Smart Med.* **2**, 20220033 (2023).
- Qasem, N. A. A., Mohammed, R. H. & Lawal, D. U. Removal of heavy metal ions from wastewater: a comprehensive and critical review. *npj Clean Water* **4**, 36 (2021).
- Long, W. et al. A novel 3D-fluorescence sensing strategy based on HN-chitosan polymer probe for rapid identification and quantification of potential adulteration in saffron. *Food Chem.* **429**, 136902 (2023).
- Pushparekha, B., Kunhanna, S., Patil, V. B. & Bikrodi Sesappa, D. Studies on characterization of blue emissive chitosan/carbazoyl biphenyl (CRB) composite films and their gamma ray irradiation mediated fluorescence quenching phenomenon. *Opt. Mater.* **138**, 113675 (2023).
- Gupta, H., Kaur, K., Singh, R. & Kaur, V. Chitosan Schiff base for the spectrofluorimetric analysis of E-waste toxins: Pentabromophenol, Fe³⁺, and Cu²⁺ ions. *Cellulose* **30**, 1381–1397 (2022).
- Li, C., Duan, L. & Cheng, X. Water-soluble chitosan-g-PMMA (PMAA)-Bodipy probes prepared by RAFT methods for the detection of Fe(3+) ion. *Carbohydr. Polym.* **299**, 120183 (2023).
- Meng, Z. et al. A naphthalimide functionalized chitosan-based fluorescent probe for specific detection and efficient adsorption of Cu(2). *Int. J. Biol. Macromol.* **239**, 124261 (2023).
- Hu, N. et al. The preparation of a chitosan-based novel fluorescent macromolecular probe and its application in the detection of hypochlorite. *Mater. Today Chem.* **29**, 101420 (2023).
- Mi, F. L. Synthesis and characterization of a novel chitosan-gelatin bioconjugate with fluorescence emission. *Biomacromolecules* **6**, 975–987 (2005).
- Geng, Z. et al. A fluorescent chitosan hydrogel detection platform for the sensitive and selective determination of trace mercury(II) in water. *J. Mater. Chem. A* **3**, 19455–19460 (2015).
- Song, J. et al. Selective determination of Cr(VI) by glutaraldehyde cross-linked chitosan polymer fluorophores. *ACS Sens.* **3**, 792–798 (2018).
- Wang, H. et al. Biomimetic enzyme cascade reaction system in microfluidic electrospray microcapsules. *Sci. Adv.* **4**, eaat2816 (2018).
- Zhao, Z. et al. Bioinspired heterogeneous structural color stripes from capillaries. *Adv. Mater.* **29**, 1704569 (2017).
- Zhang, H. et al. Natural proteins-derived asymmetric porous conduit for peripheral nerve regeneration. *Appl. Mater. Today* **27**, 101431 (2022).
- Zhang, H. et al. Protein-based hybrid responsive microparticles for wound healing. *ACS Appl. Mater. Interfaces* **13**, 18413–18422 (2021).
- Yang, Y. et al. Ordered inverse-opal scaffold based on bionic transpiration to create a biomimetic spine. *Nanoscale* **13**, 8614–8622 (2021).
- Lin, L. et al. Biomimetic epithelium/endothelium on chips. *Eng. Regen.* **3**, 201–216 (2022).
- Shao, C. et al. Polyurethane-poly pyrrole hybrid structural color films for dual-signal mechanics sensing. *Smart Med.* **1**, e20220008 (2022).
- Zhang, Z. et al. Bioinspired bilayer structural color hydrogel actuator with multi-environment responsiveness and survivability. *Small Methods* **3**, 1900519 (2019).
- Wei, X. et al. Multiplex assays of bladder cancer protein markers with magnetic structural color hydrogel microcarriers based on microfluidics. *Sens. Actuators B Chem.* **346**, 130464 (2021).
- Zhang, H. et al. Stretchable and conductive composite structural color hydrogel films as bionic electronic skins. *Adv. Sci.* **8**, 2102156 (2021).
- Zhang, H. et al. Natural polymer-derived bioscaffolds for peripheral nerve regeneration. *Adv. Funct. Mater.* **32**, 2203829 (2022).
- Zhang, H. et al. Silk fibroin hydrogels for biomedical applications. *Smart Med.* **1**, e20220011 (2022).
- Hou, J., Li, M. & Song, Y. Recent advances in colloidal photonic crystal sensors: Materials, structures and analysis methods. *Nano Today* **22**, 132–144 (2018).
- Sun, L., Chen, Z., Bian, F. & Zhao, Y. Bioinspired soft robotic caterpillar with cardiomyocyte drivers. *Adv. Funct. Mater.* **30**, 1907820 (2020).
- Luan, C. et al. Responsive photonic barcodes for sensitive multiplex bioassay. *Nanoscale* **9**, 14111–14117 (2017).
- Wang, H. et al. Enzymatic inverse opal hydrogel particles for biocatalyst. *ACS Appl. Mater. Interfaces* **9**, 12914–12918 (2017).
- Zhang, H. et al. Immunotherapeutic silk inverse opal particles for post-surgical tumor treatment. *Sci. Bull.* **65**, 380–388 (2020).
- Zhang, H. et al. Responsive drug-delivery microcarriers based on the silk fibroin inverse opal scaffolds for controllable drug release. *Appl. Mater. Today* **19**, 100540 (2020).

59. Wang, H. et al. Anisotropic structural color particles from colloidal phase separation. *Sci. Adv.* **6**, eaay1438 (2020).
60. Wang, H. et al. Oriented boronate affinity-imprinted inverse opal hydrogel for glycoprotein assay via colorimetry. *Microchim. Acta.* **187**, 348 (2020).
61. Wang, H. et al. Boronate affinity molecularly imprinted inverse opal particles for multiple label-free bioassays. *Chem. Commun.* **52**, 3296–3299 (2016).
62. Wang, H. et al. Enzyme-functionalized structural color hydrogel particles for urea detection and elimination. *J. Clean. Prod.* **315**, 128149 (2021).
63. Wang, H. et al. Responsive janus structural color hydrogel micromotors for label-free multiplex assays. *Research* **2021**, 9829068 (2021).
64. Lei, Y. et al. Functional biomaterials for osteoarthritis treatment: From research to application. *Smart Med.* **1**, e20220014 (2022).
65. Luo, Z. et al. Microfluidic electrospray photo-crosslinkable κ -Carrageenan microparticles for wound healing. *Eng. Regen.* **2**, 257–262 (2021).
66. Zhang, X. et al. Magneto-responsive microneedle robots for intestinal macromolecule delivery. *Adv. Mater.* **33**, e2104932 (2021).
67. Kuang, G., Zhang, Q., Jia, J. & Yu, Y. Freezing biological organisms for biomedical applications. *Smart Med.* **1**, e20220034 (2022).
68. Zhao, Y. et al. Multiplex detection of tumor markers with photonic suspension array. *Anal. Chim. Acta* **633**, 103–108 (2009).
69. Hu, J. et al. Photonic crystal hydrogel beads used for multiplex biomolecular detection. *J. Mater. Chem.* **19**, 5730–5736 (2009).
70. Ge, J. & Yin, Y. Responsive photonic crystals. *Angew. Chem. Int. Ed.* **50**, 1492–1522 (2011).
71. Li, Z. & Yin, Y. Stimuli-responsive optical nanomaterials. *Adv. Mater.* **31**, 1807061 (2019).
72. Li, R., Li, L., Wang, B. & Yu, L. Preparation of quantum dot-embedded photonic crystal hydrogel and its application as fluorescence sensor for the detection of nitrite. *Nanomaterials* **11**, 3126 (2021).
73. Li, H. et al. Fluorescence enhancement by heterostructure colloidal photonic crystals with dual stopbands. *J. Colloid Interface Sci.* **356**, 63–68 (2011).
74. Wu, W. et al. Carnation-like morphology of BiVO₄(4)-7 enables sensitive photoelectrochemical determination of Cr(VI) in the food and environment. *Biosensors* **12**, 130 (2022).
75. Liu, Q., Kim, J. & Cui, T. A highly sensitive photoelectrochemical sensor with polarity-switchable photocurrent for detection of trace hexavalent chromium. *Sens. Actuators B Chem.* **317**, 128181 (2020).
76. Xu, Y. et al. Cathodically pretreated AuNPs-BDD electrode for detection of hexavalent chromium. *Micromachines* **11**, 1095 (2020).
77. Breslin, C. B., Branagan, D. & Garry, L. M. Electrochemical detection of Cr(VI) with carbon nanotubes decorated with gold nanoparticles. *J. Appl. Electrochem.* **49**, 195–205 (2018).
78. Liu, S. et al. Colorimetric detection of Cr(6+) ions based on surface plasma resonance using the catalytic etching of gold nano-double cone @ silver nanorods. *Anal. Chim. Acta* **1149**, 238141 (2021).
79. Ali, S. et al. Synthesis of β -cyclodextrin grafted rhombohedral-CuO antioxidant nanozyme for detection of dopamine and hexavalent chromium through off-on strategy of peroxidase mimicking activity. *Microchem. J.* **179**, 107514 (2022).
80. Yao, C. X. et al. A visual and reversible nanoprobe for rapid and on-site determination of hexavalent chromium and lysine based on dual-emission carbon quantum dots coupled with smartphone. *Microchim. Acta.* **189**, 354 (2022).
81. Zhang, H. Y. et al. Rapid detection of Cr(VI) ions based on cobalt(II)-doped carbon dots. *Biosens. Bioelectron.* **87**, 46–52 (2017).
82. Garg, A. K. et al. Doped carbon dots for the selective sensing of hexavalent chromium in water. *J. Inst. Eng. India Ser. E* **103**, 157–165 (2020).

ACKNOWLEDGEMENTS

This work was supported by the National Natural Science Foundation of China (22302231, 82102511), the Guangdong Basic and Applied Basic Research Foundation (2023A1515011986), the Natural Science Foundation of Jiangsu (BK20210021), the Research Project of Jiangsu Province Health Committee (M2021031), the Shenzhen Fundamental Research Program (JCYJ20190808120405672), Futian Healthcare Research Project (FTWS2022013, FTWS2023080), the Fundamental Research Funds for the Central Universities, Sun Yat-sen University (23qnp153), and Clinical Trials from the Affiliated Drum Tower Hospital, Medical School of Nanjing University (2022-LCYJ-PY-05).

AUTHOR CONTRIBUTIONS

H.W. provided the idea and designed the experiment. H.S. carried out experiments and data analysis. H.S. and H.W. wrote the manuscript. H.C. and B.W. analyzed the data and revised the manuscript. L.L. and D.Z. contributed to the scientific discussion. All the authors were involved in rounds of critical revisions, and read and approved the final manuscript.

COMPETING INTERESTS

The authors declare no competing interests.

ADDITIONAL INFORMATION

Supplementary information The online version contains supplementary material available at <https://doi.org/10.1038/s41545-023-00283-5>.

Correspondence and requests for materials should be addressed to Ling Lu, Dagan Zhang or Huan Wang.

Reprints and permission information is available at <http://www.nature.com/reprints>

Publisher's note Springer Nature remains neutral with regard to jurisdictional claims in published maps and institutional affiliations.



Open Access This article is licensed under a Creative Commons Attribution 4.0 International License, which permits use, sharing, adaptation, distribution and reproduction in any medium or format, as long as you give appropriate credit to the original author(s) and the source, provide a link to the Creative Commons license, and indicate if changes were made. The images or other third party material in this article are included in the article's Creative Commons license, unless indicated otherwise in a credit line to the material. If material is not included in the article's Creative Commons license and your intended use is not permitted by statutory regulation or exceeds the permitted use, you will need to obtain permission directly from the copyright holder. To view a copy of this license, visit <http://creativecommons.org/licenses/by/4.0/>.

© The Author(s) 2023